SiliconPV: 17-20 April 2011, Freiburg, Germany

Loss analysis and improvements of industrially fabricated Cz-Si solar cells by means of process and device simulations

S. Steingrube[a]*, H. Wagner[a], H. Hannebauer[b], S. Gatz[b], Renyu Chen[c], S.T. Dunham[c], T. Dullweber[b], P.P. Altermatt[a], R. Brendel[a,b]

[a]*Leibniz University of Hannover, Institute for Solid State Physics, Dep. Solar Energy, Appelstr. 2, 30167 Hannover, Germany*
[b]*Institute for Solar Energy Research Hamelin (ISFH), Am Ohrberg 1, 31860 Emmerthal, Germany*
[c]*Department of Electrical Engineering, University of Washington, Seattle, WA 98195, USA*

Abstract

We model currently fabricated industrial-type screen-printed boron-doped Cz silicon solar cells using a combination of process and device simulations. The model reproduces the experimental results precisely and allows us to predict both the efficiency gain after specific cell improvements and the associated thermal budgets. Separating the resistive losses (evaluated for various contributions) from the recombination losses (evaluated in different device regions) allows us to forecast the improvements of the emitter and the rear side necessary such that the recombination losses in the base dominate. We predict that to increase cell efficiency considerably beyond 19.7 %, the base material needs to be improved.

© 2011 Published by Elsevier Ltd. Open access under CC BY-NC-ND license.
Selection and/or peer-review under responsibility of SiliconPV 2011

Keywords: device simulations; process simulations; Cz-Si; loss analysis; Si solar cells; solar cell improvement

1. Investigated cells and material models

By means of device and process simulations we show how models developed specifically for PV applications [e.g. 1-6] can be used to accelerate the improvement of actual solar cells. We investigate a standard screen-printed industrial type solar cell, processed on a 2.5 Ωcm boron-doped Cz-Si wafer at ISFH. We denote this cell as the *reference cell*. The textured front side of the cell is diffused by a phosphorus emitter with the profile given in Fig. 1(a) (red symbols), and electrically passivated with an PECVD deposited silicon nitride (SiN$_x$) layer. The fully metalized rear side of the cell contains an aluminum-alloyed Al-p$^+$ back surface field (BSF) with the Al profile shown in Fig. 1(b). The rear side of The cell contains no busbars.

* Corresponding author. Tel.: +49-511-762-17253 ; *E-mail address*: steingrube@solar.uni-hannover.de.
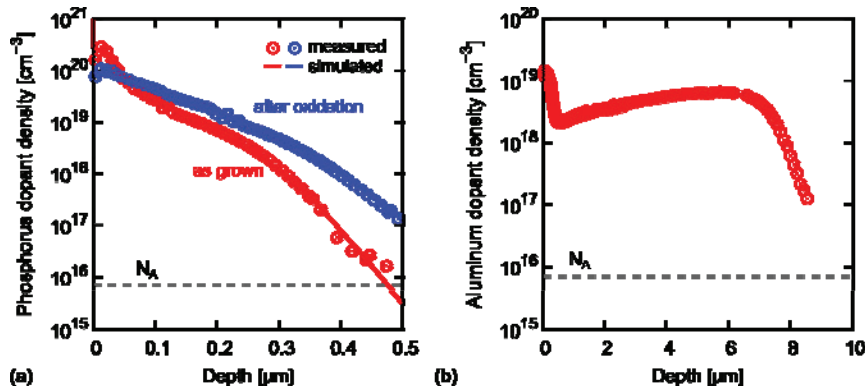
Fig. 1 (a) ECV measurements (symbols) [12] and simulations (lines) of the phosphorus emitter profiles before and after an oxidation for 15 min oxidation at 900ºC. The sheet resistivities are R_{sh}=80 Ω/□ and R_{sh}=76 Ω/□, respectively. (b) ECV measurement of the aluminum alloyed Al-p$^+$ BSF.

1. SRH lifetime in the Cz-base

In boron doped Cz-Si, the Shockley-Read-Hall (SRH) excess carrier lifetime τ_{SRH} reduces under illumination until a stable *degraded* value is reached. The SRH parameters are given by [4,7]:

$$\tau_n = 4.402024 \times 10^{39}\,\mathrm{s}\left(\frac{[\mathrm{B_s}]}{1\,\mathrm{cm^{-3}}}\right)^{-0.824}\left(\frac{[\mathrm{O_i}]}{1\,\mathrm{cm^{-3}}}\right)^{-1.748} G\,, \qquad \tau_p = 10\,\tau_n\,, \qquad E_d = E_c - 0.41\,\mathrm{eV}\,, \tag{1}$$

where $[\mathrm{B_s}] = \mathrm{N_A}$ is the substitutional boron density, $[\mathrm{O_i}] \approx 10^{17}$ to 10^{18} cm^{-3} is the interstitial oxygen density [4,8], and $G = 2$–3.5 denotes a process-related improvement factor of τ_{SRH} [4]. The asymmetric ratio of τ_p/τ_n=10 results in an injection dependent τ_{SRH}. We use $[\mathrm{O_i}] = 7 \times 10^{17}$ cm^{-3} and $G = 2.16$, yielding $\tau_n = 57.9$ μs for degraded cells, whereas $\tau_n = \tau_p$=280 μs is assumed for the non-degraded state in agreement with measurements.

1.2 SRH lifetime in the Al-p$^+$ BSF

The Al-alloyed BSF typically has measured saturation current densities $j_{0,BSF}$ between 600 fA/cm^2 and 900 fA/cm^2 [7] and can be reduced below 250 fA/cm^2 by a-Si:H passivation and annealing [9]. For the Al-profile shown in Fig. 1(b) we obtain such high values of $j_{0,BSF}$ by reducing the lifetime in the bulk region of the Al-doping [7]:

$$\frac{1}{\tau_{n,p}} = 2.8339 \times 10^{-18}\frac{1}{\mathrm{s}}\left(\frac{N_A}{1\,\mathrm{cm^{-3}}}\right)^{1.5048} f \tag{2}$$

with f < 1. We characterize the BSF via $j_{0,BSF}$, extracted from Sentaurus-Device [10] simulations of test-structures under steady-state open-circuit conditions according to Refs. [2,11]. Using f =0.007 in Eq. (2) and band-gap narrowing [1], we obtain $j_{0,BSF} = 578$ fA/cm^2.

1.3 Investigated cell designs

In the simulations, we consider three design variations of the *reference cell*. The first variation, denoted

as the *emitter cell*, refers to improvements of the emitter: a dry oxidation step is added for 15 min at 900°C so a 10–25 nm thick SiO_2 layer is formed and the phosphorus surface concentration is reduced. Hence, it is passivated with an SiO_2/SiN_x stack [12]. The profiles are reproduced with process simulations using the model of Ref. [13], see the lines in Fig. 1(a). The reduced surface dopant density leads to reduced SRH surface recombination velocity parameters [2] from $S_n = 8 \times 10^5$ cm/s for the as-grown emitter (corresponding to $j_{0,e} = 180$ fA/cm^2 via Eq.(3)), to $S_n = 2.3 \times 10^4$ cm/s (yielding $j_{0,e} = 72$ fA/cm^2 for the oxidized emitter). In a different design, we reduce the rear metalization and the BSF to 130 μm wide fingers, denoted as the *LBSF cell*. The remaining part of the rear side is passivated by an SiN_x layer. Note that surface damage underneath the SiN_x layer [14, 15, 16] is incorporated in the simulations. Finally, we apply both design variations simultaneously, denoted as the *emitter+LBSF cell*, and compare the simulation results to experiments [12]. Here, the rear side is passivated by an SiO_2/SiN_x. The resulting simulated I-V parameters are displayed in Fig. 2, and a comparison between simulated and measured values is summarized in Table 1. All simulations are shown for the degraded and the non-degraded case.

2. Loss Analysis and prediction of effects of design changes

We perform a loss analysis to understand the behavior of the different cells. In the analysis of the I-V curves, we carefully separate the resistive losses from the recombination losses.

Table 1 Comparison of measured / simulated cell parameters. The measurements of the emitter+LBSF cell are independently confirmed from Fraunhofer ISE CalLab [12] (n.s. = not specified).

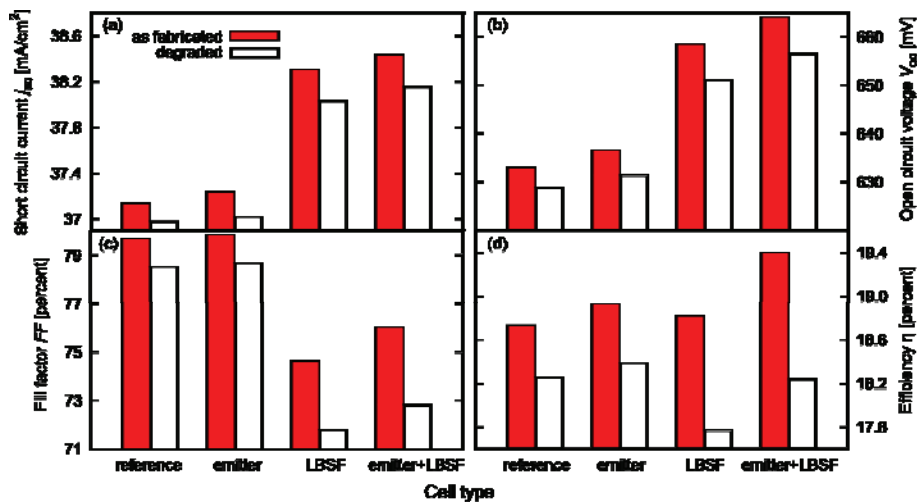| Cell-type	j_{sc} [mA/cm^2]	V_{oc} [mV]	j_{mpp} [mA/cm^2]	V_{mpp} [mV]	*FF* [%]	η [%]
reference (non-degraded)	37.3 / 37.1	633.0 / 633.0	34.9 / 35.1	536.3 / 534.1	79.4 / 79.7	18.7 / 18.7
reference (degraded)	37.1 / 37.0	628.8 / 628.9	34.9 / 34.6	527.1 / 526.9	78.8 / 78.5	18.3 / 18.3
emitter+LBSF cell (non-degraded)	38.5 / 38.4	664 / 664.0	n.s. / 36.0	n.s./ 538.8	75.8 / 76.0	19.4 / 19.4

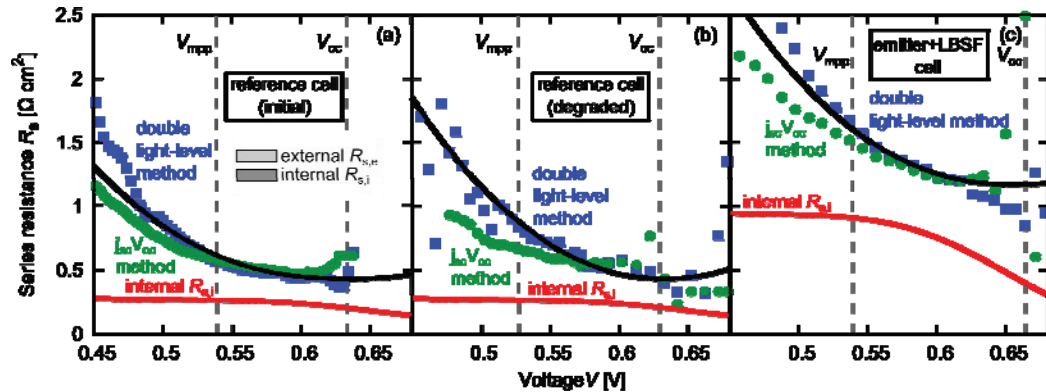Fig. 2 Simulated I-V parameters for the investigated cell designs.

Fig. 3 Lumped series resistance R_s extracted from measurements with the double light-level method (blue) and the $j_{sc}V_{oc}$ method (green) for (a) the reference cell (initial), (b) the reference cell (degraded) and (c) the LBSF cell.

2.1 Resistive losses

The lumped series resistance $R_s(V)$ is commonly extracted from the I-V curves in two different ways: either by comparing the 1-sun I-V curve with the $j_{sc}V_{oc}$ curve [17], or by comparing two illuminated I-V curves at slightly different light intensities, called the double light-level (dll) method [17, 18, 19]. Fig. 3 shows that the $j_{sc}V_{oc}$ method underestimates R_s at low V if injection-dependent effects are present, such as τ_{SRH} in degraded B-doped Cz-Si (Fig. 3(b)) or the surface recombination velocity at the rear (Fig. 3(c)). The *internal* series resistance $R_{s,i}$ from contributions in the substrate is extracted from the simulations using the dll method. The difference between $R_{s,i}$ and the lumped series resistance $R_s = R_{s,i}+R_{s,e}$ for the cell with a fully metalized rear in Fig. 3(a) and (b) is given by the *external* $R_{s,e}$ of the front metalization. For the cell with local rear contacts in Fig. 3(c), the increased internal $R_{s,i}$ originates from changes in the current-paths, and the external losses $R_{s,e}$ increase due to the variations in the rear metalization. To include $R_{s,e}$ in the simulations, we correct the simulated voltage V_{sim} by $V_{corr} = V_{sim}+R_{s,e}(V_{sim})j(V_{sim})$.

2.2 Recombination losses

The simulated recombination losses, separated into the different device components, are shown in Fig. 4 [20]. The recombination at the rear side dominates for both the reference and the emitter cell over the entire voltage range, see Fig. 4(a) and 4(b). The reduction in cell efficiency for the degraded cell, shown in Fig. 2(d), is mainly due to the reduced V_{oc} caused by the enhanced recombination in the base. Compared to the reference cell, the improved emitter in Fig. 4(b) enhances the simulated conversion efficiency only slightly because the losses in the base dominate the total losses. However, the recombination at the rear is strongly reduced in the LBSF cell in Fig. 4(c), so the emitter dominates before degradation over the entire voltage range. After degradation, recombination in the base dominates between V_{mpp} and V_{oc}. In this voltage range, the recombination rate increases sub-exponentially due to the injection dependence of the lifetime in the base, causing a reduced fill factor $FF = 71.6$ % compared to $FF = 74.6$ % for the non-degraded base, as shown in Fig. 2(c). For the emitter+LBSF cell in Fig. 4(d), the base dominates between V_{mpp} and V_{oc} for both non-degraded and degraded base material. Thus, increasing the efficiency considerably beyond 19.4 % requires an improvement of the Cz-base material. Note that the rear side passivation in Fig. 4(d) is slightly reduced compared to Fig. 4(c) due to the smaller surface charge density of $Q_f = 7\times10^{10}$ e/cm^2 for SiO$_2$ compared to $Q_f = 2.2\times10^{12}$ e/cm^2 for SiN$_x$
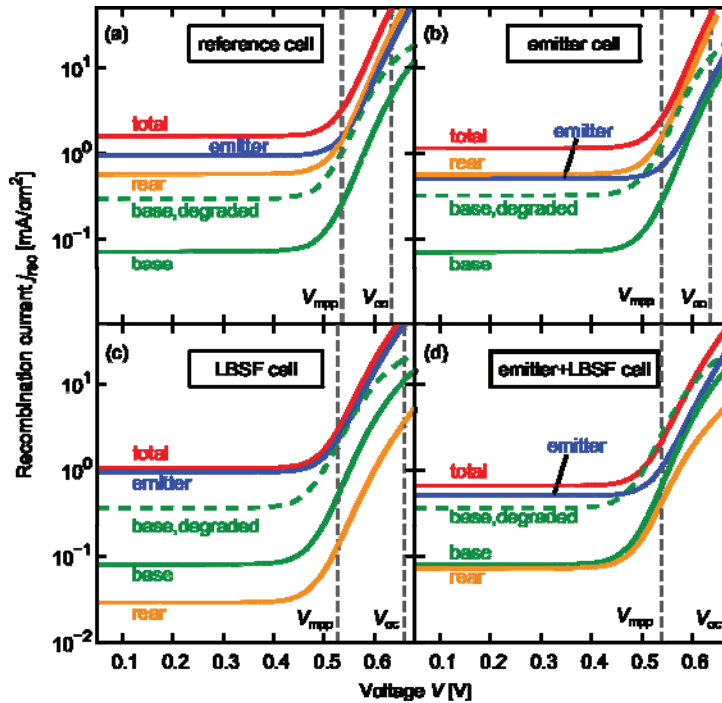
Fig. 4 The simulated recombination losses in various device regions of the different investigated cell designs before degradation. The base contribution after degradation is shown by dashed green lines for comparison. The vertical lines indicate the voltages V_{mpp} and V_{oc} for the non-degraded case.

3. Summary and outlook

We outlined an example of how device and process simulations can be used to support cell development in the laboratory. We showed that care must be taken when improving the emitter and the BSF in cells with B-doped Cz base material, because the injection dependent τ_{SRH}, measured after light-degradation, may reduce the fill factor by more than 3 % absolute compared to the non-degraded case, leading to a reduction in cell efficiency by more than 1 % absolute. We predict that a reduced external series resistance $R_{s,e}$ may improve η from the achieved 19.4% to 19.7 %, similarly as an improved emitter design [21]. The simulations show that efficiencies considerably higher than $\eta = 19.7$ % can only be achieved if the base material is improved. We forecast that for a cell with reduced external resistance $R_{s,e}$, an improved emitter, and a Ga-doped Cz-Si base with stable excess carrier lifetimes close to 800 μs after degradation [22], efficiencies of to $\eta = 20.6$ % percent may be achieved.

References

[1]   P.P. Altermatt, A. Schenk, F. Geelhaar, and G. Heiser. Reassessment of the intrinsic carrier density in crystalline silicon in view of band-gap narrowing. *J. Appl. Phys.* 2003; **93**:1598.

[2]   P.P. Altermatt, J.O. Schumacher, A. Cuevas, M. J. Kerr, S.W. Glunz, R.R. King, and G. Heiser. Numerical modeling of highly doped Si:P emitters based on Fermi–Dirac statistics and self-consistent material parameters. *J. Appl. Phys.* 2002;**92**:3187.

[3]   M. J. Kerr and A. Cuevas. General parameterization of Auger recombination in crystalline silicon. *J. Appl. Phys.* 2002; **91**:2473.

[4]   K. Bothe, R. Sinton, J. Schmidt. Fundamental Boron-Oxygen-related Carrier Lifetime Limit in Mono- and Multicrystalline Silicon. *Progress in PV* 2005;**13**:287.

[5]   S. Rein and S. W. Glunz, Electronic properties of the metastable defect in boron-doped Czochralski silicon: Unambiguous determination by advanced lifetime spectroscopy. *J. Appl. Phys.* 2003;**82**:1054 .

[6]   R. Bock, P.P. Altermatt, J. Schmidt, and R. Brendel. Formation of aluminum–oxygen complexes in highly aluminum-doped silicon. *Semic. Sci. Tech.* 2010;**25**:105007.

[7]   P. P. Altermatt, S. Steingrube, Y. Yang, C. Sprodowski, T. Dezhdar, S. Koc, B. Veith, S. Hermann, R. Bock, K. Bothe, J. Schmidt, and R. Brendel. Highly Predictive Modelling of Entire Si Solar Cells for Industrial Applications. In *Proc. 25th EPSEC* 2009, Hamburg, Germany, p. 901.

[8]   B. Lim, F. Rougieux, D. Macdonald, K. Bothe, and J. Schmidt. Generation and annihilation of boron-oxygen-related recombination centers in compensated p- and n-type silicon. *J. Appl. Phys.* 2010;**108**:103722.

[9]   R. Bock, J. Schmidt, and R. Brendel. Effective passivation of highly aluminum-doped *p*-type silicon surfaces using amorphous silicon. *Appl. Phys. Lett.* 2007; **91**:112112.

[10]   Sentaurus-Device. Synopsys Inc., Mountain View, CA. URL: www.synopsys.com/products/tcad/tcad.html.

[11]   J. O. Schumacher, P. P. Altermatt, G. Heiser, and A. G. Aberle. *Sol. Energy Mater. Sol. Cells* 2001;**65**:95.

[12]   S. Gatz, H. Hannebauer, R. Hesse, F. Werner, A. Schmidt1, T. Dullweber, J. Schmidt, K. Bothe, and R. Brendel. 19.4%-efficient large-area fully screen-printed silicon solar cells. *Phys. Status Solidi RRL* 2011;**5**:147.

[13]   S. T. Dunham. A quantitative model for the coupled diffusion of phosphorus and point defects in silicon. *J. Electrochem. Soc.* 1992;**139**:9.

[14]   S. Steingrube, P. P. Altermatt, J. Schmidt, and R. Brendel. Modelling c-Si/SiN$_x$ interface recombination by surface damage. *pss (RRL)* 2010;**4**:91.

[15]   S. Steingrube, P. P. Altermatt, D. S. Steingrube, J. Schmidt, and R. Brendel. Interpretation of recombination at c-Si/SiN$_x$ interfaces by surface damage. *J. Appl. Phys.* 2010;**108**:014506.

[16]   S. Steingrube, P. Altermatt, D. Zielke, F. Werner, J. Schmidt, and R. Brendel. Reduced passivation of silicon surfaces at low injection densities caused by H-induced defects. In *Proc. 25th EPSEC* 2010, Valencia, Spain, p. 1748.

[17]   M. Wolf and H. Rauschenbach. Series resistance effects on solar cell measurements. *Advanced Energy Conversion* 1963:455-479.

[18]   P.P. Altermatt, G. Heiser, A.G. Aberle, A. Wang, J. Zhao, S.J. Robinson, S. Bowden, and M.A. Green. Spatially resolved analysis and minimization of resistive losses in high-efficiency Si solar cells. *Prog Photovoltaics* 1996;**4**:399.

[19]   R. J. Handy. Theoretical analysis of the series resistance of a solar cell. *Solid-State Electron.* 1967;**10**:765.

[20]   A.G. Aberle, P.P. Altermatt, G. Heiser, S.J. Robinson, A. Wang, J. Zhao, U. Krumbein and M.A. Green, Limiting loss mechanisms in 23% efficient silicon solar cells, 1995, *J. Appl. Phys.* **77**:3491.

[21]   See the contribution from T. Ohrdes *et al.* at this conference.

[22]   S. W. Glunz, S. Rein, J. Knobloch, W. Wettling, and T. Abe. Comparison of boron- and gallium-doped p-type Czochralski silicon for photovoltaic application. *Prog. Photovoltaics: Res. Appl.*1999;**7**:463.